The Cryosphere Discuss., 7, 2533–2566, 2013
www.the-cryosphere-discuss.net/7/2533/2013/
doi:10.5194/tcd-7-2533-2013

The Cryosphere Discussions
Open Access

Impact of physical properties and accumulation rate on pore close-off in layered firn

S. A. Gregory, M. R. Albert, and I. Baker

Hayer School of Engineering, Dartmouth College, Hanover NH, 03766, Germany

Received: 30 April 2013 – Accepted: 2 May 2013 – Published: 13 June 2013

Correspondence to: M. R. Albert (mary.r.albert@dartmouth.edu)

Published by Copernicus Publications on behalf of the European Geosciences Union.

Abstract

Investigations into the physical characteristics of deep firn near the lock-in zone through pore close-off are needed to improve understanding of ice core records of past atmospheric concentrations. Specifically, the permeability and microstructure profiles of the firn through the diffusive column influence the entrapment of air into bubbles and thus the ice age-gas age difference. The purpose of this study is to examine the nature of pore closure processes at two polar sites with very different local temperatures and accumulation rates. Density, permeability, and microstructure measurements were made on firn cores from WAIS Divide in West Antarctica and Megadunes in East Antarctica. We found that the open pore structure plays a more important role than density in predicting gas transport properties, through the porous firn matrix. For both WAIS Divide and Megadunes, fine grained layers experience close-off shallower in the firn column than do coarse grained layers, regardless of which grain sized layer is the more dense layer at depth. Pore close-off occurs at an open porosity that is accumulation rate dependent. Low accumulation sites, with coarse grains, close-off at lower open porosities (< 10 %) than the open porosity (> 10 %) of high accumulation sites with finer grains. The depth and length of the lock-in zone is primarily dependent upon accumulation rate and microstructural variability due to differences in grain size and pore structure, rather than the density variability of the layers.

1 Introduction

As an archive for past atmospheric conditions, ice cores play an important role in understanding climate change, both natural and anthropogenic in origin. The surface of polar ice sheets is covered in a 60–120 m thick layer of firn, multiyear snow that undergoes further metamorphism with depth until it becomes solid ice at the firn-ice transition. The firn layer acts as a filter on atmospheric signals that are eventually captured within bubbles of an ice core. Because air within the firn column can exchange with the

TCD
7, 2533–2566, 2013

atmosphere until the start of the lock-in zone, where horizontal layers of firn become impermeable impeding vertical gas transport, the air entrapped in bubbles of the ice matrix is always younger than the ice (Schwander and Stauffer, 1984). Knowing the depth at which air can no longer exchange with the atmosphere is pivotal for determining the gas age/ice age difference. At present day polar sites, most studies have focused on the bulk properties of the firn and not until the recent past have studies started to include the layered nature of the firn (Albert et al., 2004; Courville et al., 2010; Freitag et al., 2004; Fujita et al., 2009; Horhold et al., 2011).

A typical firn column can be divided into three main zones based on the dominating gas transport mechanisms operating at a given depth (Sowers et al., 1992). Gas movement in the top of the firn column, the convective zone, is dominated by convection due to highly permeable firn and/or wind pumping. Below the convective zone is the diffusive zone, where the main gas transport mechanism is molecular diffusion. At the base of the diffusive zone is the non-diffusive or lock-in zone (LIZ) characterized by layers of firn, some of which are permeable and some are not. At the start of the LIZ is the lock-in depth (LID), the depth at which the first impermeable horizontal layers of firn impede vertical gas exchange with the atmosphere. The LIZ ends at the close-off depth beyond which all pores are closed-off from one another both vertically and horizontally and no gas transport exists.

A useful technique to examine firn microstructure is x-ray computed tomography. While x-ray computed tomography is well established in soil science (Taina et al., 2008), initial application to polar firn has only happened in the last 10–15 years (e.g. Coleou et al., 2001; Freitag et al., 2004; Schneebeli et al., 2004). A number of studies have been done using x-ray computed tomography to examine the microstructure of polar firn from the surface through the firn-ice transition. These studies have focused primarily on understanding how microstructure differences between fine grained and coarse grained firn influences the densification rate of polar firn (Freitag et al., 2004; Lomonaco et al., 2011; Fujita et al., 2009). Other studies include the influence of microstructure, either from thick sections or x-ray computed tomography on the permeability of firn at the top

TCD
7, 2533–2566, 2013

of the firn column (Albert et al., 2004; Courville et al., 2007; Rick and Albert, 2004). In conjunction, Courville et al. (2010) and Freitag et al. (2002) used 3-D reconstructions of firn cube microstructure to model the permeability of firn using Lattice-Boltzmann techniques. The specific influence of microstructure on bulk properties affecting gas transport in deep firn has not been well understood.

Pore close-off can be assessed through three approaches: (1) density predicted from densification models, (2) in situ through firn air measurements and modeling, and (3) laboratory-based permeability measurements. The traditional assumption is that pore close-off density is site specific, and the first layers of firn to reach this density will close-off and no longer exchange air with the atmosphere. Martinerie et al. (1992) used sixteen different sites to parameterize the mean density of pore close-off based on the temperature of the sites. Parameterizing close-off with a mean density ignores the layered nature of firn and the presence of a lock-in zone. To account for the length of the lock-in zone in firn densification modeling, Goujon et al. (2003) used a closed porosity of 37 % to indicate the close-off depth (bottom of the lock-in zone), a closed porosity of 21 % for Vostok, Antarctica, and 13 % for Summit, Greenland to indicate the lock-in depth. The length of present day lock-in zones tends to increase with an increase in accumulation rate (Landais et al., 2006). An increase in lock-in zone length at high accumulation sites has been linked by Horhold et al. (2011) to a second period of high density variability using high resolution density measurements. In this paper, using laboratory measurements, we explore the role of microstructure including pore structure on the variability of layers in deep firn and the range of depths where pore close-off occurs.

The second approach for assessing pore close-off in polar firn is through in-situ bulk firn air measurements accompanied by firn modeling. Firn air campaigns have been conducted at a number of Arctic and Antarctic sites where trace gas and isotopic fractionation are used to locate the lock-in depth. The deepest location where air can be sampled from the firn column is typically considered the close-off depth and the bottom of the lock-in zone (Clark et al., 2007; Buizert et al., 2011; Kawamura et al., 2006;

TCD
7, 2533–2566, 2013

Schwander et al., 1993; Witrant et al., 2011; Etheridge et al., 1996; Trudinger, 2001; Severinghaus et al., 2010; Severinghaus et al., 2001; Fabre et al., 2000; and Battle et al., 2011). Firn air models have been developed to construct effective diffusivity profiles through a combination of forward and inverse modeling e.g. Rommelaere et al., 1997; Trudinger et al., 1997; Buizert et al., 2011; Trudinger et al., 2002. These models use density profiles derived from densification models to obtain an open porosity profile of an individual site. The open porosity profile is then used to predict effective diffusivity profiles for various tracer gases at the site. The effective diffusivity profile is then tuned based on measurements until a good fit is found. While this method apparently works well for present day sites where firn air measurements are available, better parameterization of polar firn based on temperature and accumulation rate are needed in order to use firn air models accurately for firn columns existing in past environments. Schwander et al., 1988 demonstrated a relationship for tortuosity as a function of porosity at Siple Station, Antarctica but this relationship does not account for microstructural differences in polar firn from site to site. In an attempt to better characterize gas transport and open porosity, Freitag et al. (2002), fitted both diffusivity and permeability to open porosity using two power law functions with exponents 2.1 and 3.4 respectively for firn from Summit, Greenland. The results from Schwander et al. (1988); Fabre et al. (2000) and Freitag et al. (2002) agree reasonably well for open porosities greater than 0.2 but diverge at low porosities and none account for the layered nature of firn or density variability of the lock-in zone.

This study aims to better understand the role firn microstructure plays in controlling gas transport in deep firn and the validity of using density (bulk or local) to predict gas transport in polar firn including pore close-off by comparing firn structure from two Antarctic sites, WAIS Divide and Megadunes. Microstructural analysis, density and permeability measurements show the importance of grain and pore structure over local density and open porosity in controlling gas transport and the pore close-off process. We investigate links between accumulation rate, pore structure and gas transport properties including diffusivity and pore close-off in deep firn.

TCD
7, 2533–2566, 2013

2 Methods

2.1 Visual Stratigraphy

Stratigraphic layering of the firn was observed and recorded using a backlit light table in a cold room at the Cold Regions Research and Engineering Laboratory in Hanover, NH. Meter long core sections were placed on the light table where grain size and wind crusts were recorded to the 1mm scale. Grain size was qualitatively described using a five tier scale from coarse to fine for each meter length section. Coarse grains and fine grains were defined relative to other layers within the meter long section. Samples of 5–10 cm of similar grain size were cut for further analysis. Emphasis was put on obtaining a single homogenous layer of firn per sample whenever possible, in order to facilitate comparisons of the properties with quantitative microscopy results.

2.2 Bulk Density

Bulk density measurements were made on the same 5–10 cm resolution samples using volumetric measurements and the mass of the sample. Error in density measurements was small with less than 0.5 % standard deviation for 10 repeat measurements on a single sample. Broken or chipped pieces were not included in bulk density or permeability measurements and are not reported in this paper.

2.3 Permeability

Permeability measurements were made using the methods developed by Albert et al., 2000, and used for example in Rick and Albert, 2004, and Courville, 2007. Using a custom apparatus that had been verified on glass beads, air was drawn through a firn sample, and the associated flow rate and pressure drop across the sample were measured, along with temperature and barometric pressure. A variety of flow rates was employed. For each flow rate and associated pressure drop recorded, the permeability was obtained using Darcy's law. Flow rates of air through the samples were kept within

TCD
7, 2533–2566, 2013

the laminar flow regime where Darcy's Law holds true.

$$v = (k/\mu) \cdot (dP/dx) \quad (1)$$

Where k is the permeability constant, μ is the air viscosity, dP is the pressure differential, dx is the height of the sample and v is the flow velocity. Before measurements were taken the permeameter was calibrated using glass bead samples. Calibration was complete when measured glass bead permeability fell within the accepted literature values. Ten measurements with ten different flow rates were done on each sample and usually fell within 5–10 % of one another. At very low permeabilities fewer measurements were done on each sample due to the low flow rates needed to stay within the laminar flow regime. The lowest permeability measured was $1 \times 10^{-12} m^2$ and all samples whose measurements fell below the range of the sensitive pressure transducer were considered impermeable and assigned permeability values of $0\,m^2$.

2.4 Micro computed tomography

Firn microstructure properties were obtained using x-ray microtomography. A Skyscan 1172 model microCT was used in a cold room. Scans were run at 40 kV, a 250 µA current intensity, and a rotation step of 0.7° completing 180° rotation for each run. 275 shadow images were obtained and reconstructed using Skyscan's NRecon software for two dimensional slice reconstruction. The resolution of the images obtained is 14.8μm in which each voxel obtained represents a three dimensional cube with 14.8 µm side length. Firn samples were cut to 1cm width × 1 cm width × 1.5 cm height segments from the center of the 5 cm–10 cm samples used in density and permeability measurements. The volume of interest analyzed for microstructure properties was 538 × 538 × 673 voxels or 8 mm × 8 mm × 10 mm in size. For thresholding 256 grey levels were used and a thresholding value of 89 was set between the air and the ice phase. The large difference in linear attenuation coefficients (x-ray absorption) between ice and air enables a simple thresholding limit to be used to binarize the images. To reduce noise and minimize falsely counting incorrectly binarized voxels as pores or small ice clusters, all

TCD
7, 2533–2566, 2013

white specs less than 25 voxels surrounded by black voxels were removed and vice versa. Image analysis on both the ice phase and pore phase was done to obtain the microstructure properties of both the ice structure and pore structure of the firn sample.

The microstructural properties, derived using Skyscan's CTan software, include total porosity, open porosity, closed porosity, structural model index, surface to volume ratio, and anisotropy. The total porosity of the sample is determined by counting the total number of voxels present for the phase being analyzed and dividing that by the total number of voxels within the region of interest. Open porosity is defined as any pore that intersects with the edge of the region of interest at least once. From total and open porosity values, closed porosity of a sample can quickly be determined through subtraction. To account for closed pores that were cut during sample preparation, pore size distribution was determined for all samples where the majority of closed pores had volumes of 1 mm^3 or less. Through individual object analysis all pores with a center within 0.62 mm (the radius of a 1 mm^3 spherical pore) of the edge of the region of interest were considered closed and open porosity and closed porosity were adjusted accordingly for each sample.

Structure model index, (SMI), gives an estimation for the type of shape present in the analyzed phase. SMI values of 0, 3 and 4 correspond to an ideal plate, cylinder, and sphere respectively. Calculation of SMI follows that developed by Hildebrand et al. (1997) in which one voxel thickness is added to the surface of the phase analyzed. SMI is then calculated as follows:

$$\mathrm{SMI} = 6 \cdot (S' \cdot \mathrm{V}) / S^2 \tag{2}$$

where S' is the artificially increased surface area, S is the original surface area, and V is the initial volume of the analyzed phase. For convex shapes, SMI is positive while concave structures have negative SMI values. The surface to volume ratio, (S / V), gives the ratio of the analyzed phase surface area to the volume of the phase in three dimensions. It gives estimation of how tortuous an object is where a low S / V indicates less complexity in shape than a high S / V (Morphometric param-

TCD
7, 2533–2566, 2013

eters measured by SkyscanTM CT- analyser software, Bruker-MicroCT CT-Analyser, http://www.skyscan.be).

Anisotropy is a measure of alignment or three-dimensional symmetry within the region of interest. The value of anisotropy is determined using the mean intercept length; the length of a line traveling through an object divided by the number of times the line crosses the analyzed phase. The higher the mean intercept length the more the object is aligned in a single direction indicating a high degree of anisotropy. The mean intercept length is found at many 3-D angles within the region of interest and each MIL is plotted to create an ellipsoid. The ellipsoid is described using an orthogonal tensor whose maximum and minimum eigenvalues are used to determine the degree of anisotropy as follows:

$$DA = (1 - [\min_{eigenvalue}/\max_{eigenvalue}]) \quad (3)$$

Where the degree of anisotropy (DA) ranges from a value of 1, totally isotropic to infinity, totally anisotropic (Morphometric parameters measured by SkyscanTM CT- analyser software, Bruker-MicroCT CT-Analyser, http://www.skyscan.be).

3 Site Characteristics

3.1 Megadunes

Measurements of firn air and extraction of a firn core from a megadunes site in East Antarctica were accomplished at an undisturbed site in December 2004-January 2005 at 80.77914° S, 124.48796° E. Courville et al. (2007) thoroughly describe the site details and near-surface measurements, and Severinghaus et al. (2010) describes firn air results. The average temperature at the site is −49 °C with an accumulation rate less than 4 cm weq $\cdot$ a^{-1}. In-situ firn air measurements at Megadunes done by Severinghaus et al. (2010) indicate a LIZ from 64.5 m to 68.5 m. The convective zone at Megadunes is notably very large reaching a depth of ∼ 23 m (Severinghaus et al., 2010).

TCD
7, 2533–2566, 2013

3.2 WAIS Divide

Firn core, WDC05C, was retrieved from a previously undisturbed site at 79.46300° S 112.12317° W near the WAIS Divide ice coring site for firn air measurements in December 2005–January 2006. (Battle et al., 2011). The mean annual temperature at the site is −31 ° C and the average accumulation rate is 21 cm weq $\cdot$ a^{-1} (Banta et al., 2008). The accumulation rate and average temperature at the site are both significantly higher than those at the Megadunes location. From in-situ firn air measurements done by Battle et al. (2011) a LIZ exists from approximately 66 m to 76.54 m. Similar to other high accumulation sites, the convective zone is small, likely ranging between 1.4 m and 5.2 m in depth (Battle et al., 2011).

4 Results

While a complete bulk density profile of WAIS Divide is included, the major focus of this study was deep firn. The depth ranges of density, permeability, and microstructure we investigated for this study at each site started at 55 m, approximately ten meters above the start of the LIZ defined through firn air measurements, to a few meters below the close-off depth at each site. The deepest measurements at WAIS Divide were 78 m while the deepest measurements done at Megadunes were 75 m. Including measurements of gas transport and microstructure above the LIZ enabled examination of trends and how they relate to pore close-off in both bulk and microstructural properties. To relate relationships observed in deep firn, to firn at shallower depths, a series of permeability and density measurements were done on each core from 30–36 m. Analysis at all depths for both cores includes both fine grained and coarse grained layers.

4.1 Permeability and density

Density and permeability measurements made between 30–36 m and 55–80 m at Megadunes and WAIS Divide are displayed in Fig. 1. For both sites, the 30–36 m depths

TCD
7, 2533–2566, 2013

are many meters above the lock-in zone, and the lock-in zone falls within the 55–80 m depths. It can be seen from the overall profiles that in the 30–36 m depths above the lock-in zone, the Megadunes site is much more permeable than the WAIS Divide site. Their density profiles at this depth range are similar. In addition, it is evident that even for a given density in the 30–36 m depth range, Megadunes firn is more permeable than WAIS Divide firn, above the lock-in zone.

The relationships are different within the lock-in zone. For depths between 55–80 m just above and within the lock in zone, it can be seen from Fig. 1 that Megadunes firn is more dense than WAIS Divide but the permeability profiles are similar. Very near and within the lock-in zone, the relationship existing between density and permeability shows that Megadunes firn is more permeable for any given density than is the WAIS Divide firn. The LID, defined as the depth where multiple sequential samples are impermeable, is at 64.4 m at Megadunes and 63.8 m at WAIS Divide indicated by a red and black line respectively.

4.2 Microstructure

Microstructure imaging helps to understand the reasons for different density and permeability profiles at Megadunes and WAIS Divide. Figures 2 and 3 display three-dimensional reconstructions obtained using microcomputed tomography. The width and thickness of the reconstructed firn cubes is 8 mm while the height is 10 mm. Visually Megadunes firn (Fig. 2) has larger but less total pore space at an equivalent depth than WAIS Divide (Fig. 3). The pore structure at WAIS Divide also looks more complex and divided. For both sites, total pore space decreases and the occurrence of bubbles increases with depth.

Microstructural analysis enables quantification and validation of differences in visual observations seen between the two sites. The SMI profile, an indicator of pore shape, is the same for Megadunes and WAIS Divide with depth. The pore structure at Megadunes and WAIS Divide (Fig. 4) is primarily cylindrical at 55 m with increasing SMI, evolving to spheres towards the firn-ice transition. Surface to volume ratio

TCD
7, 2533–2566, 2013

(S / V) characterizes the complexity of a structure and can serve as a proxy for tortuosity (Spaulding et al., 2011). Megadunes firn has consistently lower values of S / V than WAIS Divide indicating a less tortuous pore structure at a given depth. S / V at Megadunes is lower than at WAIS Divide at equivalent densities as well (Fig. 4). Anisotropy profiles of both sites overlap and are almost completely isotropic. Using these microstructure parameters to describe pore structure, Megadunes and WAIS Divide pores are isotropic and evolving from cylindrical type shapes at mid-depths to spheres in deep firn. The difference occurs in tortuosity of the pore matrix, indicated by S / V, where WAIS Divide is more tortuous than Megadunes at a given depth and at a given density.

4.3 Porosity

Porosity of polar firn decreases with depth as firn densifies and serves as an indicator for the magnitude and type of gas transport present in the firn column. Total porosity of polar firn is the ratio of the air space to the ice matrix within a given volume. Total porosity is a direct reflection of density in porous media, and is generally calculated directly from the measured density of bulk samples as:

$$P = (1 - \rho/\rho_{\text{ice}}) \tag{4}$$

Where P is the porosity of the sample, ρ is the density of the sample, and ρ_{ice} is the density of pure ice ($0.917\,\text{g}\cdot\text{cm}^{-3}$). While total porosity reflects the density of a sample, open porosity gives the amount of interstitial air space available for gas transport. All pores categorized as open are assumed to connect via the complex pore network to the atmosphere. In contrast, closed porosity, gives the amount of air volume completely surrounded by ice where gas transport cannot occur. All porosity measurements in this study were derived from microcomputed tomography analysis on individual firn cubes.

Figure 5 shows that both total porosity and open porosity of Megadunes firn is consistently lower than from WAIS Divide firn at a given depth. Despite having lower open

TCD
7, 2533–2566, 2013

porosity, it is visually evident that the less-tortuous pore matrix causes Megadunes firn to be more permeable than firn at WAIS Divide at a given density. A less tortuous pore structure allows for greater air flow than if the pore structure has many twists and turns.

While total and open porosity gradually decrease with depth, closed porosity dramatically increases below the LID. Closed porosity at Megadunes and WAIS Divide is less than 8 % above the LID (Fig. 5). Below the LID, closed porosity increases and has greater variability. To understand the increase in closed porosity with no change seen in total porosity, the number and size of pores were examined. Figure 6 shows a decrease in pore size below the LID with a large increase in the total number of pores below the LID. As pore close-off progresses, WAIS Divide has more variability in the total number of pores than Megadunes within the LIZ. This is likely due to the small scale layering of firn at high accumulation sites in comparison to firn at low accumulation sites (Landais et al., 2006). For pores less than 10 mm^3, the pores at WAIS Divide tend to be smaller than those at Megadunes. For both sites, the abrupt increase in closed porosity at the LID corresponds with dissection of larger open pores in multiple locations to form many smaller closed or almost closed pores. The dissection of large open pores begins at an open porosity of ~ 8 % at Megadunes and ~ 11 % at WAIS Divide.

Another method used by Lomonaco et al. (2011) to observe the pore close-off process is the closed pore fraction (CPF) defined as the number of pores divided by the total pore volume of a given sample. Plotting CPF with depth for Megadunes and WAIS Divide, Fig. 7, shows a steady CPF of ~ 1, slightly lower for WAIS Divide, until a depth of 63 m. Below 63 m, the CPF increases with depth at a constant slope through the LIZ. While the magnitude of CPF is slightly lower in the present study, the same trend in the rate of CPF increase, was observed through the LIZ at Summit by Lomonaco et al. (2011). The increase in CPF in the LIZ of polar firn is the result of large open pores that are abruptly dissected by the ice matrix initiating the LIZ. As firn is a layered material, variability in CPF is due to microstructural differences between fine and coarse grain firn. Thus the layered nature of polar firn also dictates the depth range and size of the lock-in zone.

TCD
7, 2533–2566, 2013

5 Discussion

5.1 Application to densification models and LIZ characteristics

Pore close-off is traditionally defined in layered firn as the process in which individual layers of firn become impermeable and proceeds until all layers are impermeable or closed-off. In the current literature on pore close-off, density controls the depth at which pore close-off occurs in an individual layer and dense layers are thought to close off shallower than low density layers (Martinerie et al., 1992). Combining density driven pore close-off and noting the density cross-over observed in polar firn (Horhold et al., 2011), the first firn layers in deep firn to reach pore close-off should be the high density, coarse grained layers. Our observations of close-off including microstructure and density between Megadunes and WAIS Divide suggest that microstructure, rather than density, is the main driving force for pore close-off. At depth, Megadunes firn is consistently more dense than WAIS Divide firn yet the permeability profiles above the LID and the LID for both sites are almost identical, 64.4 m and 63.8 m respectively. To explain the lack of a direct relationship between density and permeability between Megadunes and WAIS Divide the tortuosity of the pore structure must be taken into account. Megadunes, has larger grains than WAIS Divide at a given density leading to a less tortuous pore structure causing higher permeabilities at a given density in Megadunes firn than those observed at WAIS Divide.

It should be noted that previous estimates, such as those developed by Martinerie et al. (1992) of mean pore close-off density are almost directly at the peak of a Gaussian type density distribution for all impermeable layers within the lock-in zone at each site, Fig. 8. Megadunes, a cold site with an average temperature of −49 ° C, has a predicted mean pore close-off density of 0.830 g · cm^{-3} higher than 0.821 g · cm^{-3} at WAIS Divide, a warmer site with an average temperature of −31 ° C . The density range of the distribution and length of the LIZ, are dependent upon the microstructure variability between firn layers and agree with Landais et al. (2006) who postulated that low ac-

TCD
7, 2533–2566, 2013

cumulation sites will have smaller lock-in zones from an homogenous firn column and lack of annual layering.

While comparison between two sites of significantly different local climates reveals that microstructure plays a significant role in dictating permeability and pore close-off, identifying the same trend at an individual site would further strengthen our hypothesis and constrain the impact of temperature verse accumulation rate on the process. Both Megadunes and WAIS Divide were individually analyzed by identifying fine grained and coarse grained layers within the firn column and observing their relationship with both density and permeability.

As commonly seen in polar sites, WAIS Divide firn exhibits a density cross-over in which initially high density layers consisting of fine grained firn are less dense than corresponding initially low density layers consisting of coarse grained firn. The density cross-over in Fig. 9 has been noted at WAIS Divide in high resolution density measurements on firn core WDC06A done by Kreutz et al. (2011) with a minima in density variability occurring around 30 m. In the right plot of Fig. 9, fine grained layers become impermeable shallower than coarse grained layers and a coarse grained layer is the last permeable layer of the LIZ. Therefore, despite having a lower density at depth, fine grained firn reaches pore close-off first at WAIS Divide. This implies that accumulation and near surface metamorphism resulting in either fine grained or coarse grained layers, independent of temperature, remain as identifiable features of the layers as they propagate down the column, leading to shallower pore close-off in fine grain layers at WAIS Divide.

In contrast, Megadunes does not exhibit a density cross-over and initially dense fine grained firn at surface accumulation sites on the upwind dune face remains more dense than coarse grained firn from surface hiatus sites on the leeward dune face through pore close-off (Gregory, 2013). The fine grained, dense firn originating from a past accumulation site at Megadunes becomes the first impermeable layers initiating the start of the LIZ. The ability of fine grained firn to become impermeable before coarse grained firn in this study at both WAIS Divide and Megadunes, as well as in previous studies

TCD
7, 2533–2566, 2013

(Freitag et al., 2004) regardless of whether or not it was the predominately dense layer at depth emphasizes the importance of grain size and pore structure when predicting gas transport and pore close-off in polar firn. A recent study by Horhold et al. (2011) correlated an increase in accumulation rate to an increase in density variability in deep firn leading to longer LIZs. While we agree that density variability due to layering does indeed increase for high accumulation sites, the density cross-over seen in most polar firn sites leads to an inverse relationship of density and microstructure in deep firn where fine grained layers are less dense than coarse grained layers. Because they are both based on the layering, microstructure will have high layer-to-layer variability in places where layering also makes the density variable. The microstructure variability between fine grained and coarse grained layers, likely of the same magnitude of the density variability observed by Horhold et al. (2011), controls the length of the LIZ. For polar sites, fine grained layers should reach pore close-off at shallower depths than coarse grained layers. To capture this behavior, firn densification models should include two pore close-off densities, one corresponding to the finest grained layers that will predict the LID and one corresponding to the coarsest grained layers that will predict the COD. In this way, the LID, COD, and LIZ length can be accurately estimated based on the accumulation rate of a site and the resulting microstructure variability. While Megadunes is unique due to the presence of buried antidunes, we believe that low accumulation sites should exhibit less microstructure variability in deep firn following trends of density variability developed by Horhold et al. (2011) for low accumulation sites. Separate close-off densities for fine grained and coarse grained firn should be utilized to define the LIZ in firn densification models at both high and low accumulation sites based on our observations of microstructure dependent close-off.

For a physical description of why fine grain firn reaches pore close-off first, we hypothesize that the grain size of the ice and neck size of the pore structure in firn leads to a threshold in open porosity corresponding to pore close-off in a single layer of firn. Freitag et al. (2004) found that coarse grained layers densify at a quicker rate than fine grained layers but the pore size of both layers decreased at the same rate. Therefore in

TCD
7, 2533–2566, 2013

conjunction with our findings, whichever layer has smaller pores at the surface (the fine grained layer) should close-off first. Rick and Albert (2004) and Courville et al. (2007) both found that buried layers retain evidence of their character when they were in the near-surface firn. The larger grains at Megadunes and subsequent larger pore necks enables the firn at Megadunes to reach a higher density and lower open porosity of ∼ 8 % before the open pore space is quickly dissected into many smaller closed pores. At WAIS Divide, the open porosity threshold occurs higher at ∼ 11 % open porosity, due to the smaller ice grains and smaller necks in the pore structure. For a given accumulation rate, fine grained firn will have the highest open porosity at pore close-off, coarse grained firn layers will have the lowest open porosity at pore close-off and intermediate grain size layers should have open porosity thresholds for close-off in between the two extremes. Extrapolating this relationship across a variety of accumulation rates, high accumulation rates typically lead to smaller grains and should have high open porosity (> 10 %), low density at pore close-off while low accumulation sites with larger grains should have low open porosity (< 10%), high density at pore close-off.

5.2 Application to firn air models

Increasing the understanding of how microstructure affects diffusivity in deep firn through the LIZ should decrease the necessity for inverse modeling based on present day firn air measurements within firn gas transport models. Initial diffusivity profiles within polar firn are typically modeled off the Schwander et al. (1988) parameterization of firn tortuosity as a function of porosity, despite recognition by Fabre et al. (2000) who found that tortuosity profiles are site to site dependent. A recent attempt to model permeability and diffusivity as a function of open porosity, was done by Freitag et al. (2002) on 3-D reconstructed firn cubes. The permeability constant k was fit to open porosity with the following power law:

$$k = 10^{-7.7} \cdot n_{\mathrm{op}}^{3.4} \tag{5}$$

TCD
7, 2533–2566, 2013

where n_{op} is the open porosity of the sample (Freitag et al., 2002). The power law fit allowed for permeable firn below 0.12 open porosity the threshold for permeable firn in previous studies done by Fabre et al. (2000) and Schwander et al. (1988).

Plotting permeability data for Megadunes and WAIS Divide in Fig. 10 shows high scatter around the power law fit from measured permeability for both sites, though the general curve of the power law can be seen. The power law function fails most at low open porosity values (5–10 %) at Megadunes where the firn is 200–700 % more permeable than predicted with the power law function. The large error at Megadunes is likely due to the large difference in local climate at Megadunes in comparison to the climate of Greenland where the firn in the Freitag et al. (2002) study originated. The dependence of pore structure, on grain size and accumulation rate, influences gas transport in the diffusive column along with controlling pore close-off. The low accumulation rate, large grain size, and larger less tortuous pore structure at Megadunes enables the firn to be much more permeable than predicted by Freitag et al. (2002). As WAIS Divide has a local climate much similar to Greenland, the error between modeled and measured permeability is not as large.

In deep firn it has been shown that diffusivity and permeability are linearly related (Adolph and Albert, in progress) and thus the connection between permeability and grain size/pore structure can be extrapolated to diffusivity. Firn air models that use density profiles derived from firn densification models to determine the open porosity which is then used to calculate the effective diffusivity profile of a specific gas (Buizert et al., 2012) will fall short of capturing the true nature of gas transport in deep firn. A given open porosity at a high accumulation site will lead to lower observed gas diffusivity than the diffusivity observed at a low accumulation site. The microstructure must be accounted for to improve physics based models of diffusivity in polar firn. The dependence of grain size on accumulation rate and near surface residence time observed by Albert et al. (2004); Rick and Albert (2004); Courville et al. (2007); and Fujita et al. (2009) along with an increase in gas transport due to an increase in grain size shown in this study could be used to create site specific effective open porosity profiles.

TCD
7, 2533–2566, 2013

An effective open porosity profile derived from local climate parameters, specifically accumulation rate, which captures gas transport dependence on pore structure, should improve forward firn air modeling. If the physics of forward firn air modeling can be accurately captured through climate parameters it should reduce the need for inverse modeling and enhance the reliability of forward modeling of past firn columns where inverse modeling is not plausible.

6 Conclusions

Microstructure is the main driving force for pore close-off in which fine grained firn is seen to reach pore-close off at shallower depths than coarse grained firn regardless of density. These results should be incorporated into firn densification models by the inclusion of two pore close-off densities; one for the finest grained layers which would give the LID and one for coarsest grained layers corresponding to the COD. Because they are both based on the layering, microstructure in highly-layered firn will have high variability in places where layering also makes the density variable. Thus the microstructure will have high variability in the deep firn of high accumulation sites. In relation to pore close-off, a threshold is seen in open porosity, a result of accumulation rate and near surface grain size propagating down the firn column into deep firn. At porosities lower than the threshold ($>10\,\%$ for high accumulation sites and $<10\,\%$ for low accumulation sites), closed porosity increases rapidly, total number of pores increases at a greater rate, and the size of pores dramatically decreases (many small pores opposed to a few large open pores). Parameterizing pore close-off with both grain size and density, along with the layered nature of firn in firn densification models would improve their ability to accurately predict the LID and LIZ length.

Firn air models should include an effective open porosity that accounts for differences in pore structure between high and low accumulation rate sites. An effective open porosity that reflects the pore structure of the site, not simply how much pore space is present, that correctly captures permeability in deep firn may provide better

TCD
7, 2533–2566, 2013

understanding of gas transport in the LIZ. An increase in the physical understanding of pore close-off in polar firn and its dependence upon local climate will enable more accurate modeling under firn conditions with no present day analogue constraining the gas age/ice age difference. In future work we will examine sites from a wide variety of local climates in order to further develop the dependence of gas transport and pore close-off on pore structure, grain size, and climatic condition.

Acknowledgements. This research was funded by NSF grants ANT-0944078 and IGERT-0801490. The authors thank Jeff Severinghaus, Zoe Courville and colleagues from the WAIS Divide program for useful discussions, and we thank undergraduate students Emily Harwell, Noah Pfister, and Melina Bartels for assistance with the cold room measurements.

References

Albert, M. R., Schultz, E. F., and Perron, F. E. J.: Snow and firn permeability at siple dome, Antarctica. Ann. Glaciol., 31, 353–356, 2000.

Albert, M. R., Shuman, C., Courville, Z., Bauer, R., Fahnestock, M., and Scambos, T.: Extreme firn metamorphism: Impact of decades of vapor transport on near-surface firn at a low-accumulation glazed site on the East Antarctic Plateau, Ann. Glaciol., 39, 73–78, 2004.

Adolph, A. and Albert, M. R.: The physical basis for gas transport in polar firn: a case study at Summit, Greenland in press, 2013,

Banta, J., McConnell, J., Frey, M., Bales, R., and Taylor, K.: Spatial and temporal variability in snow accumulation at the West Antarctic Ice Sheet Divide over recent centuries, J. Geophys. Res., 113, D23102, doi:10.1029/2008JD010235, 2008.

Battle, M. O., Severinghaus, J. P., Sofen, E. D., Plotkin, D., Orsi, A. J., Aydin, M., Montzka, S. A., Sowers, T., and Tans, P. P.: Controls on the movement and composition of firn air at the West Antarctic Ice Sheet Divide, Atmos. Chem. Phys., 11, 11007–11021, doi:10.5194/acp-11-11007-2011, 2011.

Buizert, C., Martinerie, P., Petrenko, V. V., Severinghaus, J. P., Trudinger, C. M., Witrant, E., Rosen, J. L., Orsi, A. J., Rubino, M., Etheridge, D. M., Steele, L. P., Hogan, C., Laube, J. C., Sturges, W. T., Levchenko, V. A., Smith, A. M., Levin, I., Conway, T. J., Dlugokencky, E. J., Lang, P. M., Kawamura, K., Jenk, T. M., White, J. W. C., Sowers, T., Schwander, J.,

TCD
7, 2533–2566, 2013

and Blunier, T.: Gas transport in firn: multiple-tracer characterisation and model intercomparison for NEEM, Northern Greenland, Atmos. Chem. Phys. Discuss., 11, 15975–16021, doi:10.5194/acpd-11-15975-2011, 2011.

Buizert, C., Martinerie, P., Petrenko, V. V., Severinghaus, J. P., Trudinger, C. M., Witrant, E., Rosen, J. L., Orsi, A. J., Rubino, M., Etheridge, D. M., Steele, L. P., Hogan, C., Laube, J. C., Sturges, W. T., Levchenko, V. A., Smith, A. M., Levin, I., Conway, T. J., Dlugokencky, E. J., Lang, P. M., Kawamura, K., Jenk, T. M., White, J. W. C., Sowers, T., Schwander, J., and Blunier, T.: Gas transport in firn: multiple-tracer characterisation and model intercomparison for NEEM, Northern Greenland, Atmos. Chem. Phys., 12, 4259–4277, doi:10.5194/acp-12-4259-2012, 2012.

Clark, I. D., Henderson, L., Chappellaz, J., Fisher, D., Koerner, R., Worthy, D. E. J., Kotzer, T., Norman, A.-L., and Barnola, J.-M.: CO_2 isotopes as tracers of firn air diffusion and age in an arctic ice cap with summer melting, devon island, canada. J. Geophys. Res., 112, D01301, doi:10.1029/2006JD007471, 2007.

Coleou, C., Lesaffre, B., Brzoska, J. B., Ludwig, W., and Boller, E.: Three-dimensional snow images by X-ray microtomography. Ann. Glaciol., 32, 75–81, 2001.

Courville, Z. R., Albert, M. R., Fahnestock, M. A., Cathles IV, L. M., and Shuman, C. A.: Impacts of an accumulation hiatus on the physical properties of firn at a low-accumulation polar site, J. Geophys. Res., 112, F02030, doi:10.1029/2005JF000429, 2007.

Courville, Z., Hörhold, M., Hopkins, M., and Albert, M.: Lattice-boltzmann modeling of the air permeability of polar firn, J. Geophys. Res., 115, F04032, doi:10.1029/2009JF001549, 2010.

Etheridge, D. M., Steele, L. P., Langenfelds, R. L., Francey, R. J., Barnola, J. M., and Morgan, V. I.: Natural and anthropogenic changes in atmospheric CO_2 over the last 1000 years from air in antarctic ice and firn, J. Geophys. Res., 101, 4115–4128, 1996.

Fabre, A., Barnola, J. M., Arnaud, L., and Chappellaz, J.: Determination of gas diffusivity in polar firn: Comparison between experimental measurements and inverse modeling, Geophys. Res. Lett., 27, 557–560, 2000.

Freitag, J., Dorbrindt, U., and Kipfstuhl, J.: A new method for predicting transport properties of polar firn with respect to gases on the pore-space scale, Ann. Glaciol., 35, 538–544, doi:10.3189/172756402781816582, 2002.

Freitag, J., Wilhelms, F., and Kipfstuhl, S.: Microstructure-dependent densification of polar firn derived from X-ray microtomography, J. Glaciol., 50, 243–250, 2004.

TCD
7, 2533–2566, 2013

Fujita, S., Okuyama, J., Hori, A., and Hondoh, T.: Metamorphism of stratified firn at dome fuji, antarctica: A mechanism for local insolation modulation of gas transport conditions during bubble close off, J. Geophys. Res., 114, F03023, doi:10.1029/2008JF001143, 2009.
Gregory, S. A.: The impact of microstructure and physical properties on pore close-off at WAIS Divide and Megadunes, MS thesis, Dartmouth College, USA, 2013.
Goujon, C., Barnola, J. M., and Ritz, C.: Modeling the densification of polar firn including heat diffusion: Application to close-off characteristics and gas isotopic fractionation for Antarctica and Greenland sites, J. Geophys. Res.-Atmos, 108, 18, 4792, doi:10.1029/2002JD003319, 2003.
Hildebrand, T. and Ruëgsegger, P.: Quantification of bone microarchitecture ?with the structure model index, Comput. Meth. Biomech. Biomed. Eng., 1, 15– 23, 1997.
Hörhold, M. W., Kipfstuhl, S., Wilhelms, F., Freitag, J., and Frenzel, A.: The densification of layered polar firn, J. Geophys. Res.-Earth Surf., 116, F01001, doi:10.1029/2009JF001630, 2011.
Kawamura, K., Severinghaus, J. P., Ishidoya, S., Sugawara, S., Hashida, G., Motoyama, H., Fujii, Y., Aoki, S., and Nakazawa, T.: Convective mixing of air in firn at four polar sites, Earth Planet Sc. Lett., 244, 672–682, 2006.
Kerbrat, M., Pinzer, B., Huthwelker, T., Gäggeler, H. W., Ammann, M., and Schneebeli, M.: Measuring the specific surface area of snow with X-ray tomography and gas adsorption: comparison and implications for surface smoothness, Atmos. Chem. Phys. Discuss., 7, 10287–10322, doi:10.5194/acpd-7-10287-2007, 2007.
Kreutz, K., Koffman, B., Breton, D., and Hamilton, G.: Microparticle, Conductivity, and Density Measurements from the WAIS Divide Deep Ice Core, Antarctica. Boulder, Colorado, USA: National Snow and Ice Data Center, doi:10.7265/N5K07264, 2011.
Landais, A., Barnola, J. M., Kawamura, K., Caillon, N., Delmotte, M., Van Ommen, T., Dreyfus, G., Jouzel, J., Masson-Delmotte, V., Minster, B., Freitag, J., Leuenberger, M., Schwander, J., Huber, C., Etheridge, D., and Morgan, V.: Firn-air delta n-15 in modern polar sites and glacial-interglacial ice: a model-data mismatch during glacial periods in antarctica?, Quaternary Sci. Rev., 25, 49–62, 2006.
Lomonaco, R., Albert, M., and Baker, I.: Microstructural evolution of fine-grained layers through the firn column at Summit, Greenland, J. Glaciol., 57, 755–762, 2011.

TCD
7, 2533–2566, 2013

Martinerie, P., Raynaud, D., Etheridge, D. M., Barnola, J. M., and Mazaudier, D.: Physical and climatic parameters which influence the air content in polar ice, Earth Planet Sc. Lett., 112, 1–13, 1992.
Rick, U., and Albert, M. R.: Firn microstructure impacts on air permeability, ERDC-CRREL Tech. Rep. TR-96, 79 pp., Cold Reg. Res. and Eng. Lab., Hanover, N. H., 2004.
Rommelaere, V., Arnaud, L., and Barnola, J. M.: Reconstructing recent atmospheric trace gas concentrations from polar firn and bubbly ice data by inverse methods, J. Geophys. Res.-Atm., 102, 30069–30083, 1997.
Schneebeli, M. and Sokratov, S. A.: Tomography of temperature gradient metamorphism of snow and associated changes in heat conductivity, Hydrol. Proc., 18, 3655–3665, 2004.
Schwander, J. and Stauffer, B.: Age difference between polar ice and the air trapped in its bubbles, Nature, 311, 45–47, 1984.
Schwander, J., Stauffer, B., and Sigg, A.: Air mixing in firn and the age of the air at pore close-off, Ann. Glaciol., 10, 141–145, 1988.
Schwander, J., Barnola, J. M., Andrie, C., Leuenberger, M., Ludin, A., Raynaud, D., and Stauffer, B.: The age of the air in the firn and the ice at summit, greenland. J. Geophys. Res.-Atmos, 98, 2831–2838, 1993.
Severinghaus, J. P., Grachev, A., and Battle, M.: Thermal fractionation of air in polar firn by seasonal temperature gradients, Geochem. Geophy. Geosy., 2, 1048, doi:10.1029/2000GC000146, 2001.
Severinghaus, J. P., Albert, M. R., Courville, Z. R., Fahnestock, M. A., Kawamura, K., Montzka, S. A., Muhle, J., Scambos, T. A., Shields, E., Shuman, C. A., Suwa, M., Tans, P., and Weiss, R. F.: Deep air convection in the firn at a zero-accumulation site, central antarctica, Earth Planet Sc. Lett., 293, 359–367, 2010.
Sowers, T., Bender, M., Raynaud, D., and Korotkevich, Y. S.: Delta-n-15 of n2 in air trapped in polar ice - a tracer of gas-transport in the firn and a possible constraint on ice age-gas age-differences. J. Geophys. Res.-Atmos, 97, 15683–15697, 1992.
Spaulding, N. E., Meese, D. A., and Baker, I.: Advanced microstructural characterization of four East Antarctic firn/ice cores, J. Glaciol., 57, 796–810, 2011.
Taina, I. A., Heck, R. J., and Elliot, T. R.: Application of X-ray computed tomography to soil science: a literature review, Can. J. Soil Sci., 88, 1–20, 2008.

TCD
7, 2533–2566, 2013

Trudinger, C. M., Enting, I. G., Etheridge, D. M., Francey, R. J., Levchenko, V. A., Steele, L. P., Raynaud, D., and Arnaud, L.: Modeling air movement and bubble trapping in firn. J. Geophys. Res.-Atmos, 102, 6747–6763, 1997.

Trudinger, C. M.: The carbon cycle over the last 1000 years inferred from inversion of ice core data, PhD thesis, Monash University, Australia, 2001.

Trudinger, C. M., Etheridge, D. M., Rayner, P. J., Enting, I. G., Sturrock, G. A., and Langenfelds, R. L.: Reconstructing atmospheric histories from measurements of air composition in firn. J. Geophys. Res.-Atm., 107, 4780, doi:10.1029/2002JD002545, 2002.

Witrant, E., Martinerie, P., Hogan, C., Laube, J. C., Kawamura, K., Capron, E., Montzka, S. A., Dlugokencky, E. J., Etheridge, D., Blunier, T., and Sturges, W. T.: A new multi-gas constrained model of trace gas non-homogeneous transport in firn: evaluation and behavior at eleven polar sites, Atmos. Chem. Phys. Discuss., 11, 23029–23080, doi:10.5194/acpd-11-23029-2011, 2011.

TCD
7, 2533–2566, 2013

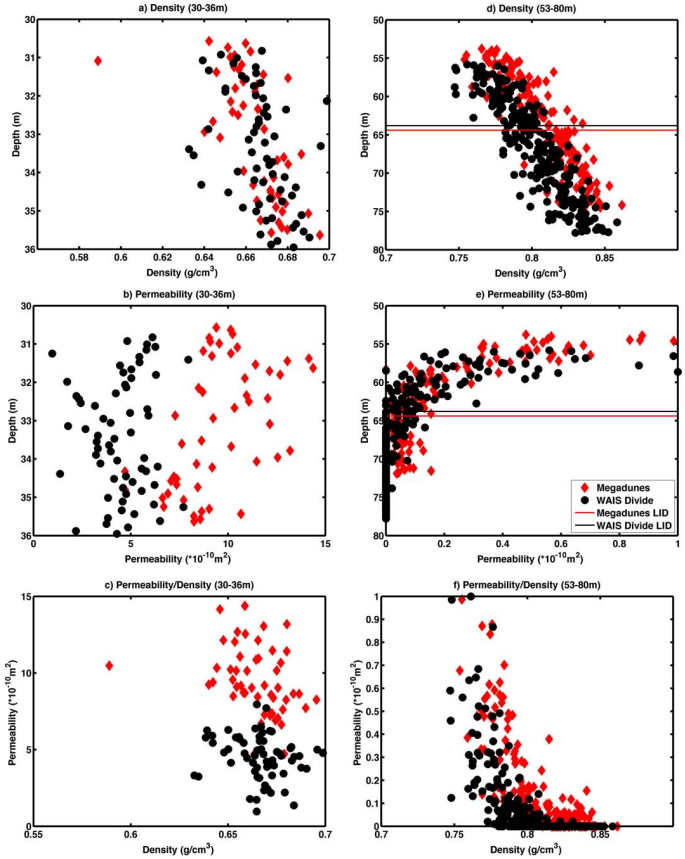

Fig. 1. (a) Density 30–36 m, **(b)** permeability 30–36 m, **(c)** density/permeability relationship 30–36 m, **(d)** density 55–80 m, **(e)** permeability 55–80 m, **(f)** density/permeability relationship 55–80 m for WAIS Divide (black circles) and Megadunes (red diamonds).

TCD
7, 2533–2566, 2013

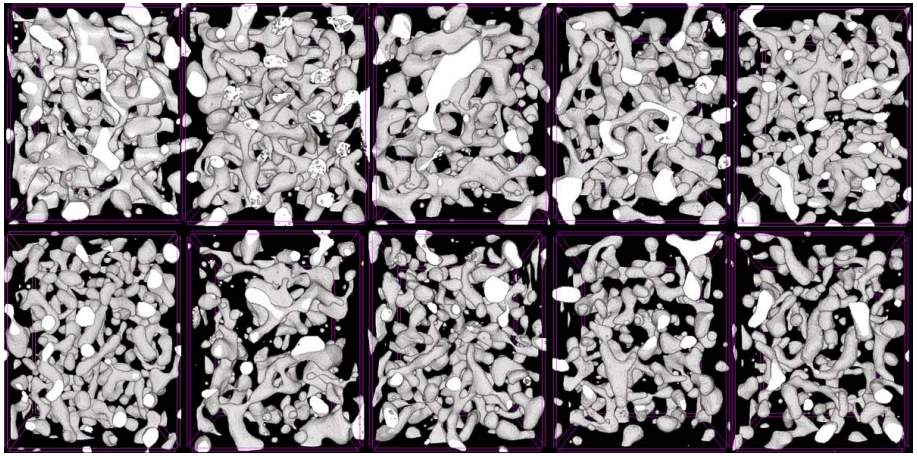

Fig. 2. Megadunes 3-D pore space reconstruction where white is the pore phase. Top row (from left to right): 56.25 m, 58.28 m, 60.43 m, 62.75 m, 64.98 m. Bottom row (from left to right): 66.79 m, 68.17 m, 70.30 m, 72.34 m, 73.27 m.

TCD
7, 2533–2566, 2013

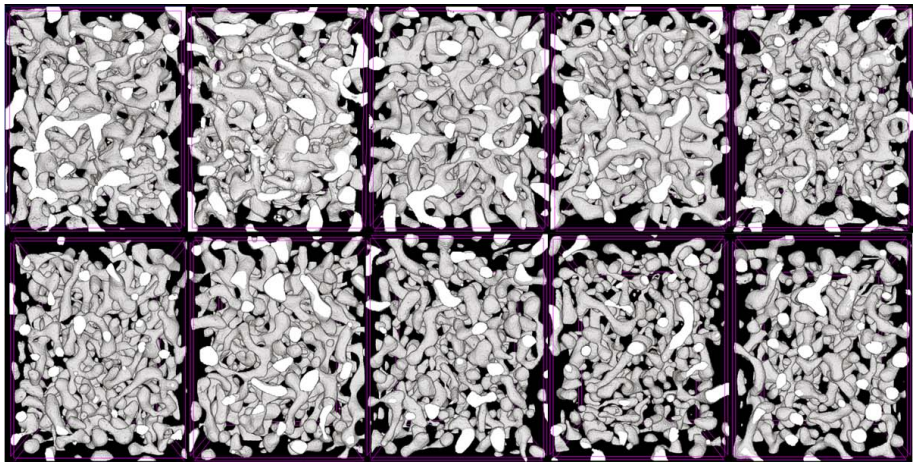

Fig. 3. WAIS Divide 3-D pore space reconstruction where white is the pore phase. Top row (from left to right): 56.36 m, 58.52 m, 60.45 m, 62.44 m, 64.61 m. Bottom row (from left to right): 66.56 m, 67.38 m, 70.56 m, 73.51 m, 74.50 m.

TCD
7, 2533–2566, 2013

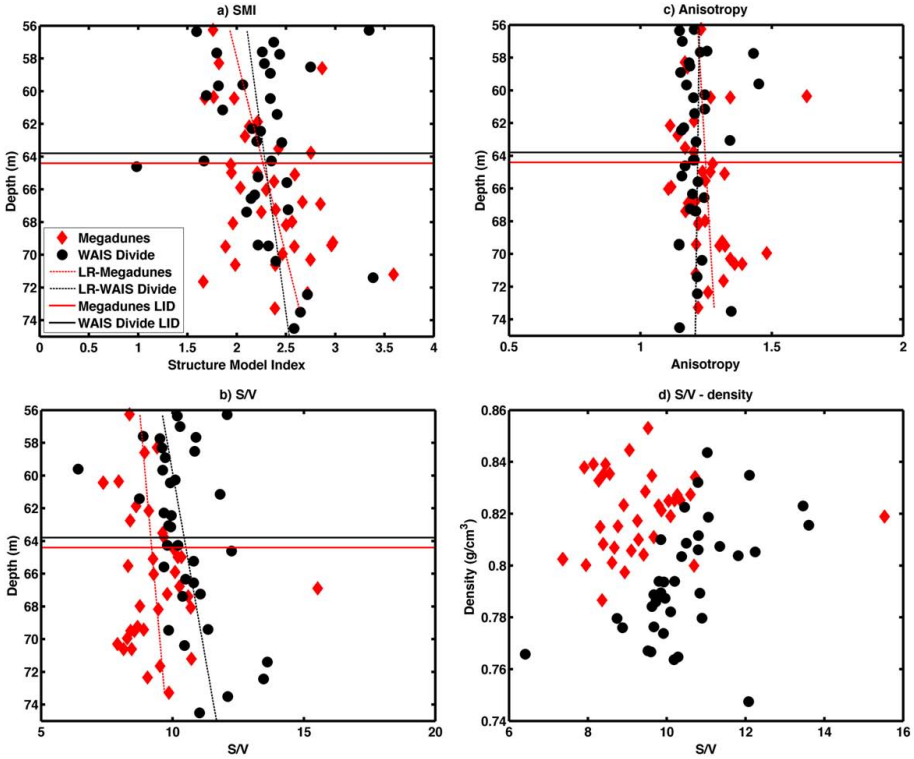

Fig. 4. (a) Structure model index, **(b)** Surface to Volume Ratio, **(c)** Anisotropy, **(d)** Surface to Volume Ratio vs Density for deep firn at Megadunes (red diamonds) and WAIS Divide (black circles).

TCD
7, 2533–2566, 2013

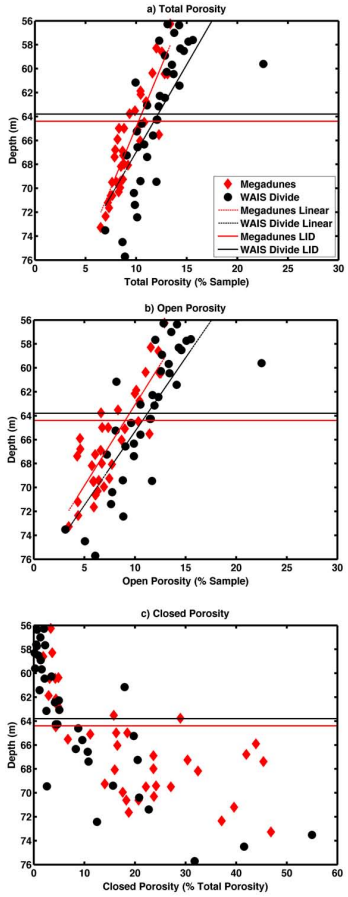

Fig. 5. (a) Total Porosity % of sample, **(b)** Open Porosity % of sample and **(c)** Closed Porosity % of total porosity for deep firn at Megadunes (red diamonds) and WAIS Divide (black circles).

TCD
7, 2533–2566, 2013

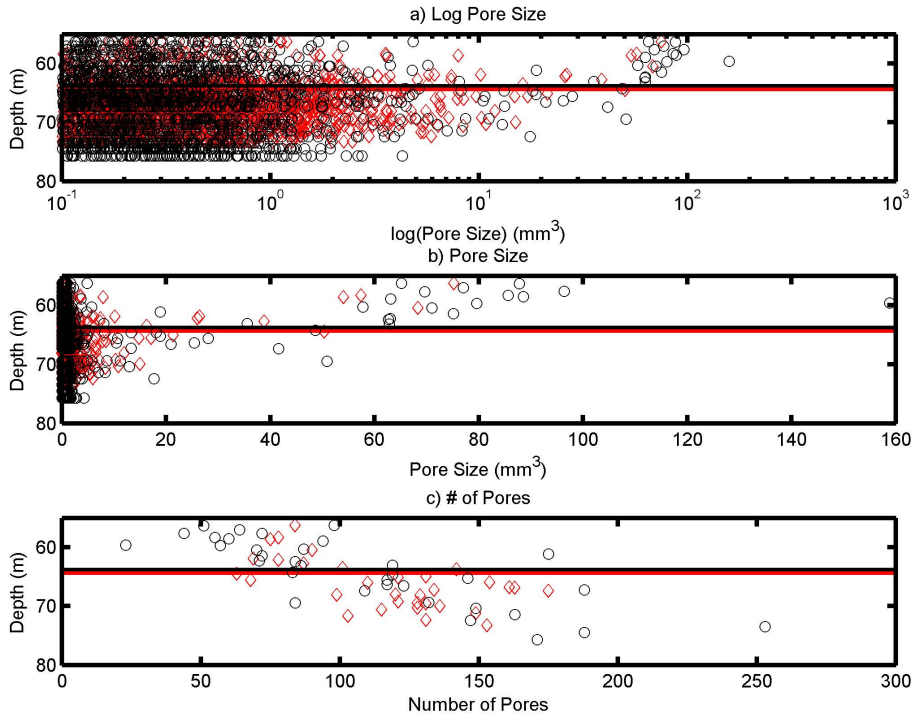

Fig. 6. a) Profiles of log pore size, b) pore size and c) number of pores for pores greater than 0.001mm^3 in deep firn, 55m to 80m, for Megadunes (red diamonds) and WAIS Divide (black circles).

TCD
7, 2533–2566, 2013

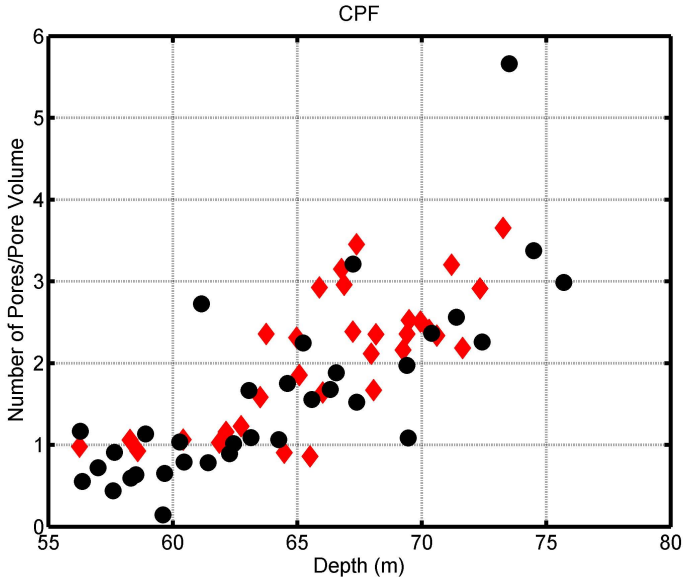

Fig. 7. Closed pore fraction (CPF) for Megadunes (red diamonds) and WAIS Divide (black circles).

TCD
7, 2533–2566, 2013

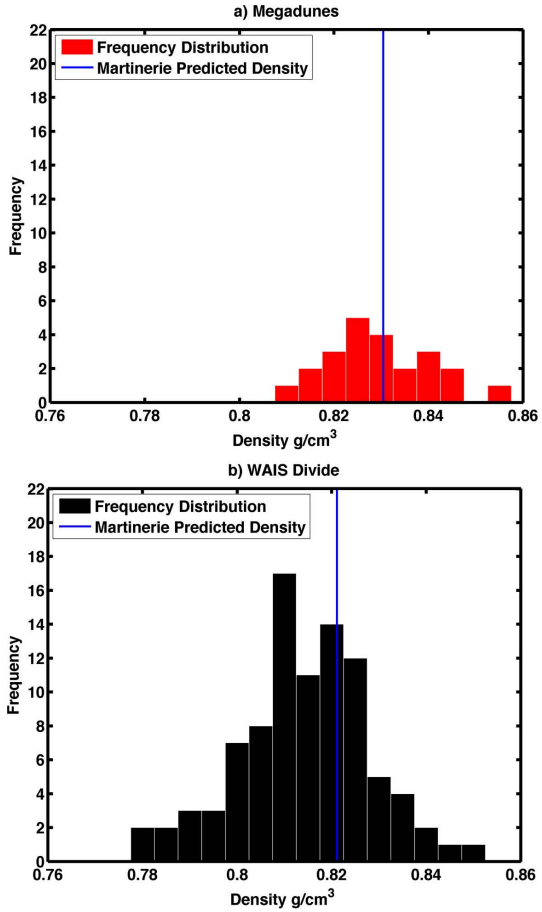

Fig. 8. Density distribution of impermeable firn samples from the LID to the end of the LIZ where all samples are impermeable at **(a)** Megadunes and **(b)** WAIS Divide.

TCD
7, 2533–2566, 2013

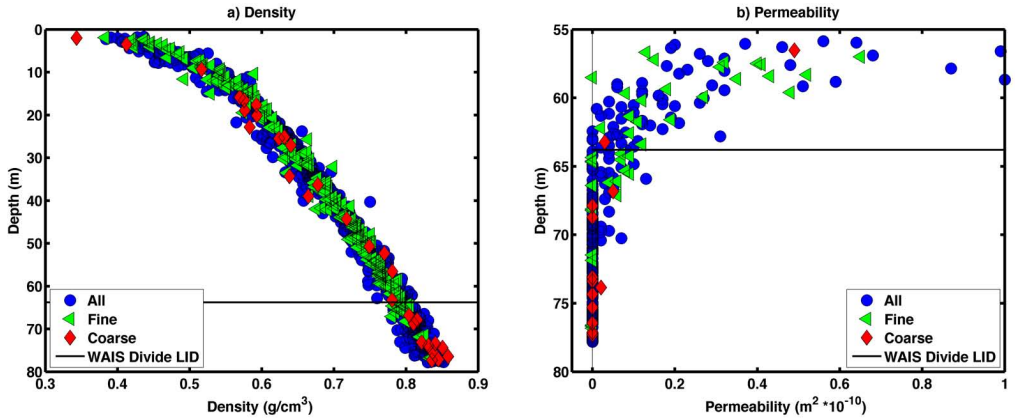

Fig. 9. (a) Density cross-over of fine and coarse grain firn at WAIS Divide and **(b)** deep firn permeability profile at WAIS Divide both show fine firn (green triangles), coarse firn (red diamonds), and intermediate firn (blue circles).

TCD
7, 2533–2566, 2013

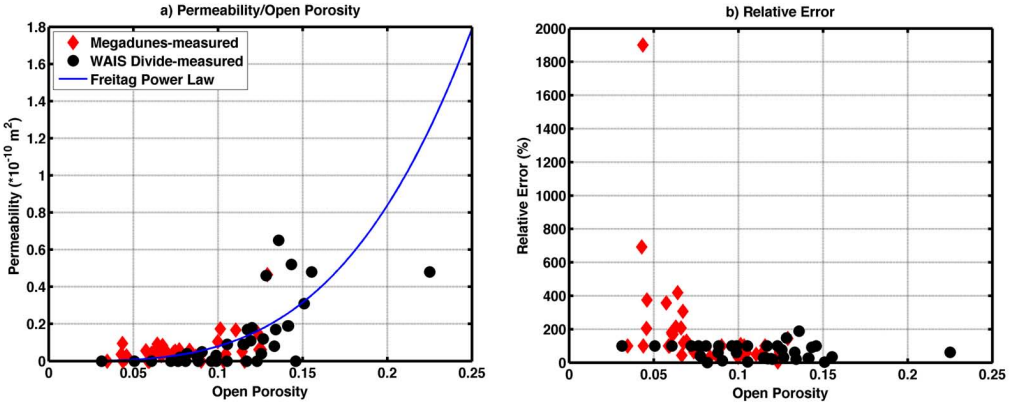

Fig. 10. (a) Measured and predicted (blue line, Freitag et al., 2002) permeability values and **(b)** relative error for Megadunes (red diamonds) and WAIS Divide (black circles).

TCD
7, 2533–2566, 2013